Low-Complexity Separate Channel Estimation for RIS-Aided MIMO Communications

Wei-Lin Chiang*, Shu-Yu Lin*, Jung-Chun Chi† and Yuan-Hao Huang*†
*Institute of Communications Engineering, †Department of Electrical Engineering, National Tsing Hua University, Taiwan.
yhhuang@ee.nthu.edu.tw

***Abstract*—Reconfigurable intelligent surface (RIS) is recently developed to enhance signal coverage and mitigate signal obstruction by altering the channel propagation environment in the MIMO communication system. The semi-passive RIS-aided MIMO system further includes some active elements in the RIS to sense the channel information and improve the channel estimation capability. By using the received signals at the RIS and base-station (BS), the compressive sensing technique can be used to estimate the channel-state-information based on the channel sparsity. This paper proposes a separate channel estimation algorithm for both user-RIS and RIS-BS channels. The matrix inverse bypass method was used to avoid massive matrix inversions in the reconstruction algorithm. Final simulation results show that the proposed algorithms achieve 10.96% and 95.73% complexity reduction for user-RIS and RIS-BS channels while still maintaining better channel estimation performance.**

***Index Terms*—Compressive sensing, Channel estimation, Reconfigurable intelligent surface.**

I. Introduction

In 5G mmWave systems, the radio wave suffers severe path loss and limited scattering, which easily causes communication blackouts in non-line-of-sight scenarios. To address these issues, reconfigurable intelligent surface (RIS) technique [1], [2] was recently proposed to solve this problem by using an array of passive reflective elements to control the phase and amplitude of radio waves, thereby focusing and directing the impinging signal beam to the receiver. Accurate channel estimation becomes one of the primary challenges to ensure the optimal reflection coefficients because the passive RIS has no baseband processing capability. Thus, the semi-passive RIS includes some active elements with RF chains to increase the channel estimation capability and reduce the channel estimation difficulty [3] [4] .

In the semi-passive RIS-aided system, active sensing nodes in RIS acquire more channel information to derive more precise beamforming and dynamic adaptation in rapidly changing environments. Although this approach increases computational complexity and pilot overhead, it significantly benefits control and performance. The least squares (LS) and linear minimum mean square error (LMMSE) RIS channel estimation requires low complexity [5] [6], but they require more training information to derive accurate channel information, leading to higher pilot overhead. The compressive sensing (CS)-based algorithm leverages the sparsity of wireless channels, so it only requires a small amount of measurement data and pilots for channel estimation. The most important of all, CS-based algorithms can derive more accurate channel information than linear methods. Thus, this paper aims to develop low-complexity CS-based separate channel estimation algorithms for semi-passive RIS-aided MIMO systems. The proposed algorithm can provide a more accurate channel estimation performance with lower computational complexity than other available algorithms.

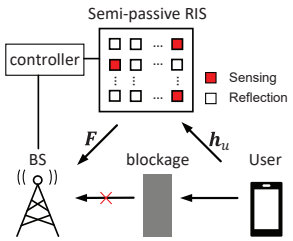

Fig. 1: The semi-passive RIS-aided communication system.

The rest of this paper is organized as follows. Section II introduces the channel estimation in the semi-passive RIS-aided MIMO system. Section III presents the proposed separate channel estimation algorithms. Section IV shows the results of estimation performance and computational complexity. Finally, Section V concludes this paper.

II. Semi-Passive RIS-Aided mmWave MIMO Systems

Figure 1 shows an RIS-aided MIMO uplink system, in which a BS with M antennas communicates with U users with single antennas and a semi-passive RIS with N reflective elements is deployed between the BS and users. The channels from the u-th user to RIS ($\mathbf{h}_u \in \mathbb{C}^{N\times 1}$) and from RIS to BS ($\mathbf{F}_u \in \mathbb{C}^{M\times N}$) are assumed to be quasi-static block-fading. Saleh-Valenzuela channel model [7] is used to simulate the sparse propagation channel and is represented by

$$\mathbf{h}_u = \sqrt{\frac{N}{L_1}} \sum_{p=1}^{L_1} \beta_{u,p}\ \mathbf{a}(\psi^{\mathrm{z}}_{u,p}, \psi^{\mathrm{y}}_{u,p}) \tag{1}$$

$$\mathbf{F} = \sqrt{\frac{MN}{L_2}} \sum_{p=1}^{L_2} \alpha_p\ \mathbf{a}(\phi^{\mathrm{z}}_{p}, \phi^{\mathrm{y}}_{p})\ \mathbf{a}^H(\theta^{\mathrm{z}}_{p}, \theta^{\mathrm{y}}_{p}) \tag{2}$$

where L_1 and L_2 are the number of paths of the user-RIS channel and RIS-BS channel, and α_p and $\beta_{u,p}$ are the

complex gains of subpaths of these two channels. Moreover, $\mathbf{a}$ represents the array steering vector, $\psi_{u,p}^{z/y}$ represents the angle of arrival (AoA) for the p-th path in the u-th user-RIS channel, $\phi_p^{z/y}$ represents the AoA of RIS-BS channel, and $\theta_p^{z/y}$ represents the angle of departure (AoD) of RIS-BS channel, where the superscript z denotes the elevation angle and y denotes the azimuth angle.The UPA steering vector of RIS is expressed by

$$\mathbf{a}(\theta,\phi)=\sqrt{\frac{1}{N_zN_y}}\ e^{j\pi\cos\theta\frac{\mathbf{n}_z}{\lambda}d}\otimes e^{j\pi\sin\theta\sin\phi\frac{\mathbf{n}_y}{\lambda}d} \quad (3)$$

where $\mathbf{n}_z=[0,1,\ldots,N_z-1]^T$ and $\mathbf{n}_y=[0,1,\ldots,N_y-1]^T$ [8]. N_z and N_y indicate the number of array elements along the z-axis and y-axis, respectively. θ and ϕ correspond to the elevation and azimuth angles, respectively. In equation (3), the symbol λ denotes the wavelength of the carrier. d represents the spacing between the antennas/reflecting elements, and it is given by $d=\frac{\lambda}{2}$. The reflection coefficients of semi-passive RIS is expressed by $\mathbf{v}=[e^{j\theta_1},...,e^{j\theta_N}]\in\mathbb{C}^{N\times 1}$. The semi-passive RIS has some active sensing elements represented by random vectorized sampling vector $\mathbf{g}(i)\in\mathbb{R}^{N\times 1}$ is 0 for $i\notin\mathbf{\Omega}$ and 1 for $\in\mathbf{\Omega}$.

A. System Model

1) User-RIS Channel Estimation: In channel estimation phase, Q subframes are used for RIS and T symbol durations are used for each user in each subframe, where $T\geq U$. We denote the reflection coefficient of the RIS in the q-th subframe as $\mathbf{v}_q$, and the orthogonal pilot sequence of the u-th user as $\mathbf{s}_u^H$. Then, the received signal at RIS in the q-th subframe becomes $\mathbf{y}_q^{\mathrm{R}}=\sum_{u=1}^{U}(\mathbf{v}_q\odot\mathbf{g}_q)^H\mathbf{h}_u\mathbf{s}_u^H+\mathbf{n}_q$, where $\mathbf{n}_q$ is noise vector. Then, the signals received from the Q subframes for all users become $\mathbf{Y}^{\mathrm{R}}=\sum_{u=1}^{U}(\mathbf{V}\odot\mathbf{G})^H\mathbf{h}_u\mathbf{s}_u^H+\mathbf{N}$, where $\mathbf{V}=[\mathbf{v}_1,...,\mathbf{v}_Q]\in\mathbb{C}^{N\times Q}$, $\mathbf{G}=[\mathbf{g}_1,...,\mathbf{g}_Q]\in\mathbb{R}^{N\times Q}$, $\mathbf{N}=[\mathbf{n}_1,...,\mathbf{n}_Q]\in\mathbb{C}^{Q\times T}$.Using the pilot sequence orthogonality, the u-th user received signal is

$$\widetilde{\mathbf{y}_u^{\mathrm{R}}}=\frac{1}{\sigma_p^2T}\mathbf{Y}^{\mathrm{R}}\mathbf{s}_u=(\mathbf{V}\odot\mathbf{G})^H\mathbf{h}_u+\widetilde{\mathbf{n}_u}. \quad (4)$$

Then, the user-RIS channel estimation problem is

$$\widehat{\mathbf{h}_u}=\arg\min_{\mathbf{h}_u}\|\widetilde{\mathbf{y}_u^{\mathrm{R}}}-(\mathbf{V}\odot\mathbf{G})^H\mathbf{h}_u\|_2^2,\ \text{for } u=1,...,U. \quad (5)$$

2) RIS-BS Channel Estimation: The received signal at the BS in the q-th subframe is $\mathbf{Y}_q^{\mathrm{B}}=\sum_{u=1}^{U}\mathbf{F}\,\mathrm{diag}(\mathbf{h}_u)\mathbf{v}_q\mathbf{s}_u^H+\mathbf{W}_{q,u}$. By utilizing the pilot sequence orthogonality, the u-th user's received signal is $\mathbf{y}_{q,u}^{\mathrm{B}}=\frac{1}{\sigma_p^2T}\mathbf{Y}_q^{\mathrm{B}}\mathbf{s}_u=\mathbf{F}\,\mathrm{diag}(\mathbf{h}_u)\mathbf{v}_q+\widetilde{\mathbf{w}_{q,u}}$. The u-th user's received signals in Q subframes is

$$\widetilde{\mathbf{Y}_u^{\mathrm{B}}}=[\mathbf{y}_{1,u}^{\mathrm{B}},\mathbf{y}_{2,u}^{\mathrm{B}},..,\mathbf{y}_{Q,u}^{\mathrm{B}}]=\mathbf{F}\ \mathrm{diag}(\mathbf{h}_u)\mathbf{V}+\widetilde{\mathbf{W}_u} \quad (6)$$

where $\widetilde{\mathbf{W}_u}=[\widetilde{\mathbf{w}_{1,u}},\widetilde{\mathbf{w}_{2,u}},...,\widetilde{\mathbf{w}_{Q,u}}]\in\mathbb{C}^{M\times Q}$ is the noise matrix. The received signals of all users in Q subframes becomes

$$\widetilde{\mathbf{Y}^{\mathrm{B}}}=\mathbf{F}[\mathrm{diag}(\mathbf{h}_1)\mathbf{V},\mathrm{diag}(\mathbf{h}_2)\mathbf{V},...,\mathrm{diag}(\mathbf{h}_U)\mathbf{V}]+\widetilde{\mathbf{W}}. \quad (7)$$

The RIS-BS channel estimation can be expressed as

$$\widehat{\mathbf{F}_u}=\arg\min_{\mathbf{F}}\|\widetilde{\mathbf{Y}_u^{\mathrm{B}}}-\mathbf{F}\mathrm{diag}(\mathbf{h}_u)\mathbf{V}\|_F^2. \quad (8)$$

The final estimated channel is the average of all solutions from all users' reflected signals. This can be expressed as

$$\widehat{\mathbf{F}}=\frac{1}{U}\sum_{u=1}^{U}\widehat{\mathbf{F}_u}. \quad (9)$$

B. Problem Reformulation with Virtual Angular Channel

To exploit the channel sparsity for CS-based channel estimation, we can express the u-th user-RIS and RIS-BS channels by $\mathbf{h}_u\approx\mathbf{A}_t\boldsymbol{\zeta}_u$ and $\mathbf{F}\approx\mathbf{A}_r\Xi\mathbf{A}_t^H$, respectively, where $\mathbf{A}_t\in\mathbb{C}^{N\times G_t}$ is the dictionary of the RIS's AoA/AoD, $\mathbf{A}_r\in\mathbb{C}^{M\times G_r}$ is the dictionary of the BS's AoA, G_t is the dictionary size of RIS's AOA/AoD, and G_r is the dictionary size of BS's AoA. The $\boldsymbol{\zeta}_u\in\mathbb{C}^{G_t\times 1}$ and $\mathbf{\Xi}\in\mathbb{C}^{G_r\times G_t}$ are the approximate sparse angular channels.The dictionary $\mathbf{A}_t$ and $\mathbf{A}_r$ can be expressed as follows [8]

$$\mathbf{A}_t=[\mathbf{a}(\theta_1,\phi_1),..,\mathbf{a}(\theta_1,\phi_{\kappa\sqrt{N}}),..,\mathbf{a}(\theta_{\kappa\sqrt{N}},\phi_{\kappa\sqrt{N}})] \quad (10)$$

$$\mathbf{A}_r=[\mathbf{a}(\theta_1,\phi_1),..,\mathbf{a}(\theta_1,\phi_{\kappa\sqrt{M}}),..,\mathbf{a}(\theta_{\kappa\sqrt{M}},\phi_{\kappa\sqrt{M}})] \quad (11)$$

where κ is the oversampling rate. The user-RIS channel estimation problem becomes

$$\widehat{\boldsymbol{\zeta}_u}=\arg\min_{\boldsymbol{\zeta}_u}\|\boldsymbol{\zeta}_u\|_0,\ \text{s.t. }\|\widetilde{\mathbf{y}_u^{\mathrm{R}}}-\mathbf{\Phi}\boldsymbol{\zeta}_u\|_2^2<\epsilon \quad (12)$$

where $\mathbf{\Phi}=(\mathbf{V}\odot\mathbf{G})^H\mathbf{A}_t$, ϵ is the tolerance, and the reconstructed channel of u-th user can be stated as $\widehat{\mathbf{h}_u}=\mathbf{A}_t\widehat{\boldsymbol{\zeta}_u}$. Similarly, the RIS-BS channel estimation can be expressed as

$$\widehat{\mathbf{\Xi}}=\arg\min_{\mathbf{\Xi}}\|\mathbf{\Xi}\|_0,\ \text{s.t. }\|\widetilde{\mathbf{Y}^{\mathrm{B}}}-\mathbf{A}_r\mathbf{\Xi}\widehat{\ddot{\mathbf{\Theta}}}\|_F^2<\epsilon, \quad (13)$$

where $\widehat{\ddot{\mathbf{\Theta}}}=[\mathrm{diag}(\widehat{\mathbf{h}}_1)\mathbf{V},\mathrm{diag}(\widehat{\mathbf{h}}_2)\mathbf{V},\ldots,\mathrm{diag}(\widehat{\mathbf{h}}_U)\mathbf{V}]$, and $\widehat{\mathbf{h}}_u$ is the estimated user-RIS channel vector obtained from backhaul link. Then, we apply the tensor mode-n product property, and the problem can be formulated as

$$\widehat{\mathbf{\Xi}}=\arg\min_{\mathbf{\Xi}}\|\mathbf{\Xi}\|_0,\ \text{s.t. }\|\widetilde{\mathbf{Y}^{\mathrm{B}}}-\mathbf{\Xi}\times_1\mathbf{A_r}\times_2\widehat{\ddot{\mathbf{\Theta}}}^H\|_F^2<\epsilon, \quad (14)$$

Finally, the RIS-BS channel can derived by $\widehat{\mathbf{F}}=\mathbf{A}_r\widehat{\mathbf{\Xi}}\mathbf{A}_t^H$.

III. Proposed Channel Estimation Algorithms

A. User-RIS Channel Estimation

The look ahead orthogonal matching pursuit (LAOMP) [9] was presented to improve the performance of orthogonal matching pursuit (OMP) by using the look ahead strategy to obtain better performance. For each iteration, LAOMP selects L atoms in the sensing matrix $\mathbf{\Phi}$ with the least matching residual in remaining candidate atoms. In LAOMP algorithm, the time-consuming step is to calculate pseudo inverse of selected atom matrix $\mathbf{\Phi}_{\mathcal{I}_k}$ from the dictionary $\mathbf{\Phi}$ in the k-th iteration which is shown in [9].

$$\mathbf{z}_k=\mathbf{\Phi}_{\mathcal{I}_k}^{\dagger}\mathbf{y}=(\mathbf{\Phi}_{\mathcal{I}_k}^H\mathbf{\Phi}_{\mathcal{I}_k})^{-1}\ \mathbf{\Phi}_{\mathcal{I}_k}^H\mathbf{y}=\mathbf{G}_{\mathcal{I}_k,\mathcal{I}_k}^{-1}\mathbf{\Phi}_{\mathcal{I}_k}^H\mathbf{y} \quad (15)$$

where $\mathbf{G}_{\mathcal{I}_k,\mathcal{I}_k} = \mathbf{\Phi}_{\mathcal{I}_k}^H \mathbf{\Phi}_{\mathcal{I}_k} \in \mathbb{C}^{|\mathcal{I}_k|\times|\mathcal{I}_k|}$. We apply the Schur-Banachiewicz block-wise matrix inverse [10] to realize the pseudo inverse of matrix $\mathbf{\Phi}_{\mathcal{I}_k}$ Then, the reformulated solution in the k-th iteration of LAOMP can be expressed as

$$\begin{aligned}\mathbf{z}_k &= \mathbf{G}_{\mathcal{I}_k,\mathcal{I}_k}^{-1} \mathbf{\Phi}_{\mathcal{I}_k}^H \mathbf{y} \\ &= \begin{bmatrix} \mathbf{G}_{I_{k-1},I_{k-1}}^{-1} + V\mathbf{A}^H\mathbf{A} & -V\mathbf{A}^H \\ -V\mathbf{A} & V \end{bmatrix} \begin{bmatrix} \mathbf{\Phi}_{\mathcal{I}_{k-1}}^H \mathbf{y} \\ \mathbf{\Phi}_{i_k}^H \mathbf{y} \end{bmatrix} \\ &= \begin{bmatrix} \mathbf{z}_{k-1} + V\mathbf{A}^H Q \\ -VQ \end{bmatrix},\end{aligned} \tag{16}$$

where $\mathbf{A} = \mathbf{G}_{i_k,\mathcal{I}_{k-1}} \mathbf{G}_{\mathcal{I}_{k-1},\mathcal{I}_{k-1}}^{-1}$, $V = \frac{1}{\mathbf{G}_{i_k,i_k} - \mathbf{A}\mathbf{G}_{\mathcal{I}_{k-1},i_k}}$ and $Q = \mathbf{A}\mathbf{\Phi}_{\mathcal{I}_{k-1}}^H \mathbf{y} - \mathbf{\Phi}_{i_k}^H \mathbf{y}$. Besides, the matching term $\boldsymbol{\alpha}_k$ can be rewritten as

$$\boldsymbol{\alpha}_k = \mathbf{\Phi}^H \mathbf{r}_k = \boldsymbol{\alpha}_{k-1} - \mathbf{G}_{\mathcal{I}_k} \begin{bmatrix} V\mathbf{A}^H M \\ -VM \end{bmatrix}, \tag{17}$$

where $\boldsymbol{\alpha}_{k-1} = \mathbf{\Phi}^H \mathbf{y} - \mathbf{\Phi}^H \mathbf{\Phi}_{\mathcal{I}_{k-1}} \mathbf{z}_{k-1}$, and $\mathbf{G}_{\mathcal{I}_k} = \mathbf{\Phi}^H \mathbf{\Phi}_{\mathcal{I}_k}$. The pseudo-inverse matrix $\mathbf{G}_{\mathcal{I}_k,\mathcal{I}_k}^{-1}$, $\mathbf{z}_k$ and $\boldsymbol{\alpha}_k$ are iteratively updated based on the results in the previous iteration, thereby avoiding matrix inversion and reducing complexity. The complete MIB-LAOMP algorithm is summarized in **Algorithm 1** along with the residual updating subfunction in **Algorithm 2**.

Algorithm 1 Matrix Inverse Bypass Look Ahead Orthogonal Matching Pursuit (MIB-LAOMP)

Input: sensing matrix $\mathbf{\Phi} \in \mathbb{C}^{Q\times G_t}$, $\mathbf{G} = \mathbf{\Phi}^H\mathbf{\Phi} \in \mathbb{C}^{G_t\times G_t}$,measurement vector $\mathbf{y} \in \mathbb{C}^Q$, target sparsity K, look ahead parameter $L \le K$.

Output: reconstructed signal $\boldsymbol{\zeta}_u \in \mathbb{C}^{G_t}$, where $\boldsymbol{\zeta}_u(\mathcal{I}) = \mathbf{z}_K$. $\mathbf{n} = [n_1, ..., n_L]^T$, $\mathbf{j} = [j_1, ..., j_L]^T$.

Initialization
1) $\mathbf{z}_0 = 0$;
2) $\boldsymbol{\alpha}_0 = \mathbf{\Phi}^H\mathbf{y}$;
3) $\mathcal{I} = \emptyset$;
4) $\mathbf{j} \leftarrow$ indices of the L largest values of $\boldsymbol{\alpha}_0$;
5) **for** $l = 1, 2, ..., L$ **do**
6) $\quad \mathbf{n}(l) =$ **MIB-LA-Residual** $(\mathbf{\Phi}, \mathbf{G}, \mathbf{y}, \mathbf{z}_0, \boldsymbol{\alpha}_0, \mathcal{I}_0, \mathbf{j}(l))$;
7) **end for**
8) $l = \arg\min_l |\mathbf{n}(l)|$;
9) $i_1 = \mathbf{j}(l)$;
10) $\mathcal{I}_1 = \mathcal{I}_0 \cup i_1$;
11) $\mathbf{\Phi}_{\mathcal{I}_1} = \mathbf{\Phi}(:, \mathcal{I}_1)$;
12) $\mathbf{G}_{\mathcal{I}_1,\mathcal{I}_1}^{-1} = \frac{1}{\mathbf{\Phi}_{\mathcal{I}_1}^H \mathbf{\Phi}_{\mathcal{I}_1}} = \frac{1}{\mathbf{G}_{\mathcal{I}_1,\mathcal{I}_1}}$
13) $\mathbf{z}_1 = \mathbf{G}_{\mathcal{I}_1,\mathcal{I}_1}^{-1} \mathbf{\Phi}_{\mathcal{I}_1}^H \mathbf{y}$;
14) $\boldsymbol{\alpha}_1 = \boldsymbol{\alpha}_0 - \mathbf{G}_{\mathcal{I}_1}\mathbf{z}_1$;
15) $k = 1$;
repeat
$\quad k = k + 1$;
$\quad \mathbf{j} \leftarrow$ indices of the L largest values of $\boldsymbol{\alpha}_{k-1} \notin \mathcal{I}_{k-1}$;
$\quad$ **for** $l = 1, 2, ..., L$ **do**
$\quad\quad \mathbf{n}(l) =$ **MIB-LA-Residual**$(\mathbf{\Phi}, \mathbf{G}, \mathbf{y}, \mathbf{z}_{k-1}, \boldsymbol{\alpha}_{k-1}, \mathcal{I}_{k-1}, \mathbf{j}(l))$;
$\quad$ **end for**
$\quad l = \arg\min_l |\mathbf{n}(l)|$;
$\quad i_k = \mathbf{j}(l)$;
$\quad \mathcal{I}_k = \mathcal{I}_{k-1} \cup i_k$;
$\quad \mathbf{A} = \mathbf{G}_{i_k,\mathcal{I}_{k-1}} \mathbf{G}_{\mathcal{I}_{k-1},\mathcal{I}_{k-1}}^{-1}$
$\quad \mathbf{V} = \frac{1}{\mathbf{G}_{i_k,i_k} - \mathbf{A}\mathbf{G}_{\mathcal{I}_{k-1},i_k}}$
$\quad \mathbf{Q} = \mathbf{A}\mathbf{\Phi}_{\mathcal{I}_{k-1}}^H \mathbf{y} - \mathbf{\Phi}_{i_k}^H \mathbf{y}$
$\quad \mathbf{G}_{\mathcal{I}_k,\mathcal{I}_k}^{-1} = \begin{bmatrix} \mathbf{G}_{\mathcal{I}_{k-1},\mathcal{I}_{k-1}}^{-1} + \mathbf{V}\mathbf{A}^H\mathbf{A} & -\mathbf{V}\mathbf{A}^H \\ -\mathbf{V}\mathbf{A} & \mathbf{V} \end{bmatrix}$
$\quad \mathbf{z}_k = \begin{bmatrix} \mathbf{z}_{k-1} + \mathbf{V}\mathbf{A}^H\mathbf{Q} \\ -\mathbf{V}\mathbf{Q} \end{bmatrix}$
$\quad \boldsymbol{\alpha}_k = \boldsymbol{\alpha}_{k-1} - \mathbf{G}_{\mathcal{I}_k} \begin{bmatrix} \mathbf{V}\mathbf{A}^H\mathbf{Q} \\ -\mathbf{V}\mathbf{Q} \end{bmatrix}$;
until $(k \ge K)$

Algorithm 2 Matrix Inverse Bypass Look Ahead Residual (MIB-LA-Residual)

Input: sensing matrix $\mathbf{\Phi} \in \mathbb{C}^{Q\times G_t}$, $\mathbf{G} = \mathbf{\Phi}^H\mathbf{\Phi} \in \mathbb{C}^{G_t\times G_t}$, target sparsity K, measurement vector $\mathbf{y} \in \mathbb{C}^Q$, previous reconstructed signal $\mathbf{z}_{k-1}$, previous matching term $\boldsymbol{\alpha}_{k-1}$, previous support set $\mathcal{I}_{k-1}$, new chosen index i_k.

Output: norm of residual $n = \|\mathbf{y} - \mathbf{\Phi}_{\mathcal{I}_K}\mathbf{z}_K\|_2 \in \mathbb{R}$.

Initialization
1) $\mathbf{A} = \mathbf{G}_{i_k,\mathcal{I}_{k-1}} \mathbf{G}_{\mathcal{I}_{k-1},\mathcal{I}_{k-1}}^{-1}$
2) $\mathbf{V} = \frac{1}{\mathbf{G}_{i_k,i_k} - \mathbf{A}\mathbf{G}_{\mathcal{I}_{k-1},i_k}}$
3) $\mathbf{Q} = \mathbf{A}\mathbf{\Phi}_{\mathcal{I}_{k-1}}^H \mathbf{y} - \mathbf{\Phi}_{i_k}^H \mathbf{y}$
4) $\mathcal{I}_k = \mathcal{I}_{k-1} \cup i_k$;
5) $\mathbf{G}_{\mathcal{I}_k,\mathcal{I}_k}^{-1} = \begin{bmatrix} \mathbf{G}_{\mathcal{I}_{k-1},\mathcal{I}_{k-1}}^{-1} + \mathbf{V}\mathbf{A}^H\mathbf{A} & -\mathbf{V}\mathbf{A}^H \\ -\mathbf{V}\mathbf{A} & \mathbf{V} \end{bmatrix}$
6) $\mathbf{z}_k = \begin{bmatrix} \mathbf{z}_{k-1} + \mathbf{V}\mathbf{A}^H\mathbf{Q} \\ -\mathbf{V}\mathbf{Q} \end{bmatrix}$
7) $\boldsymbol{\alpha}_k = \boldsymbol{\alpha}_{k-1} - \mathbf{G}_{\mathcal{I}_k} \begin{bmatrix} \mathbf{V}\mathbf{A}^H\mathbf{Q} \\ -\mathbf{V}\mathbf{Q} \end{bmatrix}$;
8) $k = |\mathcal{I}_k|$;
repeat
$\quad k = k + 1$;
$\quad i_k = \arg\max_{i_k} |\mathbf{a}_{k-1}(i_k)|$;
$\quad \mathcal{I}_k = \mathcal{I}_{k-1} \cup i_k$;
$\quad \mathbf{A} = \mathbf{G}_{i_k,\mathcal{I}_{k-1}} \mathbf{G}_{\mathcal{I}_{k-1},\mathcal{I}_{k-1}}^{-1}$
$\quad \mathbf{V} = \frac{1}{\mathbf{G}_{i_k,i_k} - \mathbf{A}\mathbf{G}_{\mathcal{I}_{k-1},i_k}}$
$\quad \mathbf{Q} = \mathbf{A}\mathbf{\Phi}_{\mathcal{I}_{k-1}}^H \mathbf{y} - \mathbf{\Phi}_{i_k}^H \mathbf{y}$
$\quad \mathbf{G}_{\mathcal{I}_k,\mathcal{I}_k}^{-1} = \begin{bmatrix} \mathbf{G}_{\mathcal{I}_{k-1},\mathcal{I}_{k-1}}^{-1} + \mathbf{V}\mathbf{A}^H\mathbf{A} & -\mathbf{V}\mathbf{A}^H \\ -\mathbf{V}\mathbf{A} & \mathbf{V} \end{bmatrix}$
$\quad \mathbf{z}_k = \begin{bmatrix} \mathbf{z}_{k-1} + \mathbf{V}\mathbf{A}^H\mathbf{Q} \\ -\mathbf{V}\mathbf{Q} \end{bmatrix}$
$\quad \boldsymbol{\alpha}_k = \boldsymbol{\alpha}_{k-1} - \mathbf{G}_{\mathcal{I}_k} \begin{bmatrix} \mathbf{V}\mathbf{A}^H\mathbf{Q} \\ -\mathbf{V}\mathbf{Q} \end{bmatrix}$;
until $(k \ge K)$

B. RIS-BS Channel Estimation

In the RIS-BS angular virtual channel, the RIS directs the users' signals to the BS through a common channel; therefore, the channel from the RIS to the BS shares a common sparse structure across different users. Thus, we adopted the n-way block orthogonal matching pursuit (N-BOMP) reconstruction [11] to leverage the joint sparsity of the channel and tensor compressive sensing approach to reduce complexity. The tensor $\boldsymbol{\mathcal{Z}}$ is then reconstructed by solving the associated minimization problem

$$\boldsymbol{\mathcal{Z}} = \arg\min_{\boldsymbol{\mathcal{Z}}} \|\boldsymbol{\mathcal{Y}} - \boldsymbol{\mathcal{Z}} \times_1 \boldsymbol{\Phi}_{\mathcal{I}_k^1} \times_2 \boldsymbol{\Phi}_{\mathcal{I}_k^2}\|_F^2, \tag{18}$$

Where we represent BS received signal matrix and sparse channel matrix in tensor form, $\boldsymbol{\mathcal{Z}} = \boldsymbol{\Xi}$ and $\boldsymbol{\mathcal{Y}} = \widetilde{\mathbf{Y}^{\mathrm{B}}}$, mode-n equivalent sensing matrix is dereved by $\boldsymbol{\Phi}_{\mathcal{I}_k^1} = \mathbf{A}_r$ and $\boldsymbol{\Phi}_{\mathcal{I}_k^2} = \hat{\tilde{\boldsymbol{\Theta}}}^H$

However, the original N-BOMP can include incorrect atoms in the support set when the block sparsity property is not satisfied. To resolve this problem, we propose the matrix inverse bypass multi-residual n-way block orthogonal matching pursuit (MIB-MR-N-BOMP) in **Algorithm** 3.

The multi-residual, inspired by the look-ahead strategy, is utilized in Step 6 to Step 15 of the loop section. We only check the L atoms that are most likely in the matching term. This method ensures that the selected atoms contribute to the minimum residual in the reconstructed signal. This mechanism reduces the risk of selecting incorrect atoms, which can otherwise propagate errors through the block sparsity structure. Moreover, the MIB technique is also used to reduce the computational burden of pseudo-inverse calculation similar to the MIB-LAOMP algorithm. Thus, the MIB-MR-N-BOMP algorithm can ensure accurate signal reconstruction with reduced computational complexity.

Algorithm 3 Matrix Inverse Bypass Multi-residual N-way Block Orthogonal Matching Pursuit (MIB-MR-N-BOMP)

Input: mode-n equivalent sensing matrix $\{\boldsymbol{\Phi}_1, \boldsymbol{\Phi}_2\}$, with $\boldsymbol{\Phi}_n \in \mathbb{C}^{I_n \times M_n}$, $n = 1, 2$, measurement tensor $\boldsymbol{\mathcal{Y}} \in \mathbb{C}^{I_1 \times I_2}$, $\mathbf{G}_n = \boldsymbol{\Phi}_n^H \boldsymbol{\Phi}_n \in \mathbb{C}^{I_n \times M_n}$, $n = 1, 2$, multiple residual parameter L, sparsity K.

Output: estimated signal in sparse domain $\boldsymbol{\mathcal{Z}} \in \mathbb{C}^{M_1 \times M_2}$.

Initialization
1) $\mathcal{I}_0^n = \emptyset$, $n = 1, 2$;
2) $\boldsymbol{\mathcal{R}}_0 = \boldsymbol{\mathcal{Y}}$;
3) $\boldsymbol{\mathcal{C}}_0 = \boldsymbol{\mathcal{R}}_0 \times_1 \boldsymbol{\Phi}_1^H \times_2 \boldsymbol{\Phi}_2^H$;
4) $\mathbf{F}(l^1, l^2) = |\boldsymbol{\mathcal{C}}_0(l^1, l^2)|$;
5) $\mathbf{m}^n \leftarrow$ indices of the L largest values of $\mathbf{F}$ such that $\mathbf{m}^n \notin \mathcal{I}_{k-1}^n$, $n = 1, 2$.
6) **for** $i = 1, 2, ..., L$ **do**
7) $\quad \mathcal{J}^n = \mathcal{I}_{k-1}^n \cup \mathbf{m}^n(i)$, $n = 1, 2$;
8) $\quad \boldsymbol{\Phi}_{\mathcal{J}^n} = \boldsymbol{\Phi}_n(:, \mathcal{J}^n)$, $n = 1, 2$;
9) $\quad \mathbf{G}^{-1}_{\mathcal{J}^n, \mathcal{J}^n} = \frac{1}{\boldsymbol{\Phi}^H_{\mathcal{J}^n}, \boldsymbol{\Phi}_{\mathcal{J}^n}} = \frac{1}{\mathbf{G}_{\mathcal{J}^n}}$, $n = 1, 2$.
10) $\quad \widetilde{\boldsymbol{\mathcal{Z}}}_i = \boldsymbol{\mathcal{Y}} \times_1 (\mathbf{G}^{-1}_{\mathcal{J}^1, \mathcal{J}^1} \boldsymbol{\Phi}^H_{\mathcal{J}^1}) \times_2 (\mathbf{G}^{-1}_{\mathcal{J}^2, \mathcal{J}^2} \boldsymbol{\Phi}^H_{\mathcal{J}^2})$;
11) $\quad \widetilde{\boldsymbol{\mathcal{R}}} = \boldsymbol{\mathcal{Y}} - \widetilde{\boldsymbol{\mathcal{Z}}}_i \times_1 \boldsymbol{\Phi}_{\mathcal{J}^1} \times_2 \boldsymbol{\Phi}_{\mathcal{J}^2}$;
12) $\quad \mathbf{r}(i) = \sum_{l^1=1}^{I_1} \sum_{l^2=1}^{I_2} |\widetilde{\boldsymbol{\mathcal{R}}}(l^1, l^2)|$;
13) **end for**
14) $j \leftarrow$ index of the lowest values of $\mathbf{r}$;
15) $\mathcal{I}_1^n = \mathcal{I}_0^n \cup \mathbf{m}^n(j)$, $n = 1, 2$;
16) $\boldsymbol{\Phi}_{\mathcal{I}_1^n} = \boldsymbol{\Phi}(:, \mathcal{I}_1^n)$, $n = 1, 2$.
17) $\mathbf{G}^{-1}_{\mathcal{I}_1^n, \mathcal{I}_1^n} = \frac{1}{\boldsymbol{\Phi}^H_{\mathcal{I}_1^n}, \boldsymbol{\Phi}_{\mathcal{I}_1^n}}$, $n = 1, 2$.
18) $\boldsymbol{\mathcal{Z}}_1 = \widetilde{\boldsymbol{\mathcal{Z}}}_j$;
19) $\boldsymbol{\mathcal{R}} = \boldsymbol{\mathcal{Y}} - \boldsymbol{\mathcal{Z}}_1 \times_1 \boldsymbol{\Phi}_{\mathcal{I}_1^1} \times_2 \boldsymbol{\Phi}_{\mathcal{I}_1^2}$.
20) $\boldsymbol{\mathcal{C}}_1 = \boldsymbol{\mathcal{R}} \times_1 \boldsymbol{\Phi}_1^H \times_2 \boldsymbol{\Phi}_2^H$;
21) Iteration counter $k = 1$;

2: **repeat**
3: $\quad k = k + 1$;
4: $\quad \mathbf{F}(l^1, l^2) = |\boldsymbol{\mathcal{C}}_{k-1}(l^1, l^2)|$;
5: $\quad \mathbf{m}^n \leftarrow$ indices of the L largest values of $\mathbf{F}$ such that $\mathbf{m}^n \notin \mathcal{I}_{k-1}^n$, $n = 1, 2$
6: $\quad$ **for** $i = 1, 2, ..., L$ **do**
7: $\quad\quad j^n = \mathbf{m}^n(i)$, $n = 1, 2$;
8: $\quad\quad \mathcal{J}^n = \mathcal{I}_{k-1}^n \cup j^n$, $n = 1, 2$;
9: $\quad\quad \mathbf{A}_n = \mathbf{G}_{j^n, \mathcal{I}_{k-1}^n} \mathbf{G}^{-1}_{\mathcal{I}_{k-1}^n, \mathcal{I}_{k-1}^n}$, $n = 1, 2$;
10: $\quad\quad \mathbf{V}_n = \frac{1}{\mathbf{G}_{j^n, j^n} - \mathbf{A}_n \mathbf{G}_{\mathcal{I}_{k-1}^n, j^n}}$, $n = 1, 2$;
11: $\quad\quad \mathbf{G}^{-1}_{\mathcal{J}^n, \mathcal{J}^n} = \begin{bmatrix} \mathbf{G}^{-1}_{\mathcal{I}_{k-1}^n, \mathcal{I}_{k-1}^n} + \mathbf{V}_n \mathbf{A}_n^H \mathbf{A}_n & -\mathbf{V}_n \mathbf{A}_n^H \\ -\mathbf{V}_n \mathbf{A}_n & \mathbf{V}_n \end{bmatrix}$, $n = 1, 2$;
12: $\quad\quad \widetilde{\boldsymbol{\mathcal{Z}}}_i = \boldsymbol{\mathcal{Y}} \times_1 (\mathbf{G}^{-1}_{\mathcal{J}^1, \mathcal{J}^1} \boldsymbol{\Phi}^H_{\mathcal{J}^1}) \times_2 (\mathbf{G}^{-1}_{\mathcal{J}^2, \mathcal{J}^2} \boldsymbol{\Phi}^H_{\mathcal{J}^2})$;
13: $\quad\quad \widetilde{\boldsymbol{\mathcal{R}}} = \boldsymbol{\mathcal{Y}} - \widetilde{\boldsymbol{\mathcal{Z}}}_i \times_1 \boldsymbol{\Phi}_{\mathcal{J}^1} \times_2 \boldsymbol{\Phi}_{\mathcal{J}^2}$;
14: $\quad\quad \mathbf{r}(i) = \sum_{l^1=1}^{I_1} \sum_{l^2=1}^{I_2} |\widetilde{\boldsymbol{\mathcal{R}}}(l^1, l^2)|$;
15: $\quad$ **end for**
16: $\quad j \leftarrow$ index of the lowest values of $\mathbf{r}$;
17: $\quad i_k^n = \mathbf{m}^n(j)$, $n = 1, 2$;
18: $\quad \mathcal{I}_k^n = \mathcal{I}_{k-1}^n \cup i_k^n$, $n = 1, 2$;
19: $\quad \mathbf{A}_n = \mathbf{G}_{i_k^n, \mathcal{I}_{k-1}^n} \mathbf{G}^{-1}_{\mathcal{I}_{k-1}^n, \mathcal{I}_{k-1}^n}$, $n = 1, 2$;
20: $\quad \mathbf{V}_n = \frac{1}{\mathbf{G}_{i_k^n, i_k^n} - \mathbf{A}_n \mathbf{G}_{\mathcal{I}_{k-1}^n, i_k^n}}$, $n = 1, 2$;
21: $\quad \mathbf{G}^{-1}_{\mathcal{I}_k^n, \mathcal{I}_k^n} = \begin{bmatrix} \mathbf{G}^{-1}_{\mathcal{I}_{k-1}^n, \mathcal{I}_{k-1}^n} + \mathbf{V}_n \mathbf{A}_n^H \mathbf{A}_n & -\mathbf{V}_n \mathbf{A}_n^H \\ -\mathbf{V}_n \mathbf{A}_n & \mathbf{V}_n \end{bmatrix}$, $n = 1, 2$;
22: $\quad \boldsymbol{\mathcal{Z}}_k = \widetilde{\boldsymbol{\mathcal{Z}}}_j$
23: $\quad \boldsymbol{\mathcal{R}} = \boldsymbol{\mathcal{Y}} - \boldsymbol{\mathcal{Z}}_k \times_1 \boldsymbol{\Phi}_{\mathcal{I}_k^1} \times_2 \boldsymbol{\Phi}_{\mathcal{I}_k^2}$;
24: $\quad \boldsymbol{\mathcal{C}}_k = \boldsymbol{\mathcal{R}} \times_1 \boldsymbol{\Phi}_1^H \times_2 \boldsymbol{\Phi}_2^H$;
25: **until** $\left(|\mathcal{I}_k^1||\mathcal{I}_k^2| \geq K\right)$
26: $\boldsymbol{\mathcal{Z}}(\mathcal{I}^1, \mathcal{I}^2) = \boldsymbol{\mathcal{Z}}_K$;

IV. Simulation Results and Complexity Analysis

We simulated the RIS-aided MIMO system with $M = 36$, $N = 64$, $U = 8$, $T = 8$, and active sensing node ratio of η=50%. The AoA and AoD are uniformly distributed over the intervals $[-\pi/2, \pi/2]$ and $[-\pi, \pi]$, respectively. An oversampling rate of $\kappa = 4$ was used to design the dictionary. The iteration numbers of K were 16 and 128 for the MIB-

LAOMP and MIB-MR-N-BOMP, respectively. Normalized mean square error (NMSE) values were calculated by averaging 1000 channel realizations of SNR = [-10, -5, 0, 5, 10] (dB).

A. Channel Estimation Performance Analysis

1) Effect of Measurement Number on Channel Estimation Performance: The illustration in Figure 2 shows the simulation of average channel estimation performance with varying numbers of measurements. Figure 2(a) demonstrates the user-RIS channel estimation, while Figure 2(b) depicts the RIS-BS channel estimation. The results indicate that the NMSE of the channel estimation for both channels decreases as the number of measurements increases. In Figure 2(a), the simulation results with $Q = 16$ show that, even with increasing SNR, this number of measurements is insufficient to accurately reconstruct the channel, resulting in a significant performance gap compared to $Q = 32$. Under conditions where Q exceeds 32, the performance of LAOMP generally surpasses that of OMP. This improvement can be attributed to LAOMP's look ahead mechanism, which is designed to evaluate multiple potential paths and select the optimal one. Conversely, in Figure 2(b), the channel estimation is improved by jointly processing all users' signals reflected through the RIS to the BS. This joint processing enhances the estimation performance through an averaging effect, and it is evident that the NMSE decreases with increasing SNR for different numbers of measurements Q in the simulation results.

2) Evaluation of estimation results with different methods: Figure 3 shows the user-RIS channel estimation results with $Q = 64$ subframes. It is evident that the proposed MIB-LAOMP has better performance than SAMP [12], CoSaMP [13] and OMP algorithms. Figure 4 shows the RIS-BS channel estimation results. When $Q = 32$, both the N-BOMP [11] and MIB-MR-N-BOMP algorithms outperform the two-stage simultaneous LAOMP (TS-SLAOMP) [14] when the SNR value exceeds 0 dB. The primary reason is that the block sparsity assumption of the N-BOMP-based algorithms matches with the common sparsity property of the RIS-BS channel. The MIB-MR-N-BOMP has a significant performance advantage in the high SNR region because the multiple residual process leads to reliable index selection results. In the simulations under the conditions of Q = 64 and SNR = 10 dB, the proposed MIB-MR-N-BOMP achieves an NMSE of 0.0011, which is significantly lower than the TS-SLAOMP [14] by 75%.

3) Computational Complexity Analysis: Figure 5 shows the computational complexity of different algorithms for the user-RIS channel estimation. The MIB-LAOMP has much lower complexity than that of the LAOMP because the matrix inverse operation is avoided in the MIB-LAOMP. For a dictionary size $G_t = 1024$, the MIB-LAOMP has a significant complexity reduction of approximately 10.96%. Figure 6 shows the computational complexity of different algorithms for the RIS-BS channel estimation. The proposed MR-N-BOMP algorithm exhibits lower computational complexity than TS-SLAOMP [14] because, during channel reconstruction, the TS-

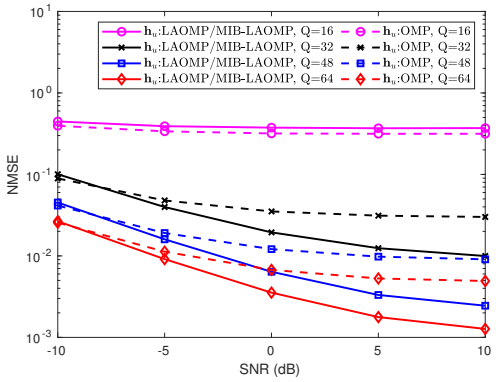

(a) user-RIS channel.

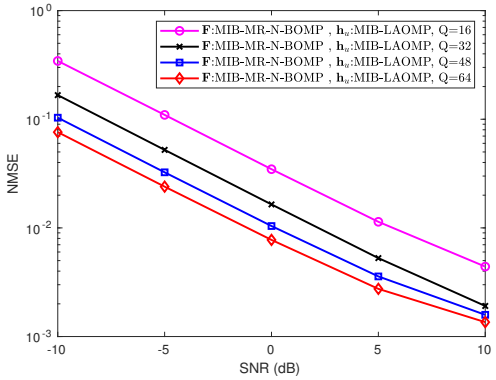

(b) RIS-BS channel.

Fig. 2: Evaluation of estimation results with different number of measurements.

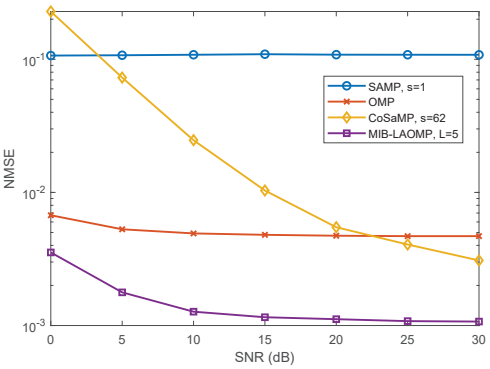

Fig. 3: The user-RIS channel estimation results .

SLAOMP transforms the compressive sensing problem into a 1D Kronecker-based CS model, which leads to an equivalent sensing matrix with significantly larger dimensions. With the dictionary sizes of $G_t = 1024$ and $G_r = 576$, the proposed MR-N-BOMP yields substantial complexity reduction of approximately 95.73%.

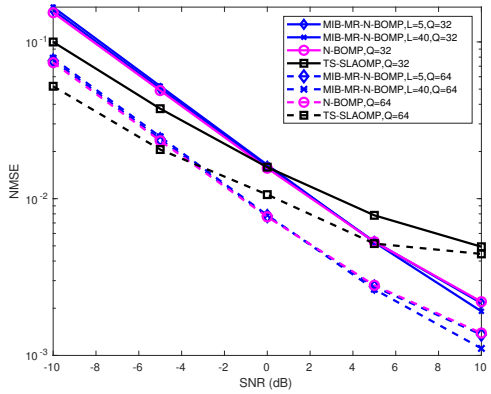

Fig. 4: The RIS-BS channel estimation results.

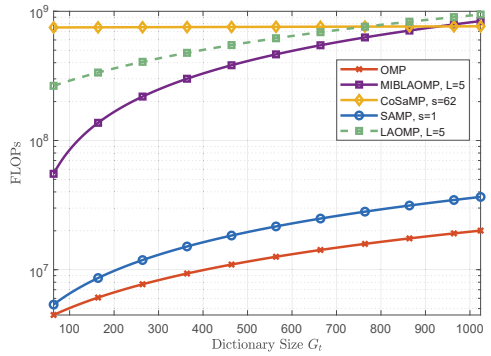

Fig. 5: Complexity of user-RIS channel estimations.

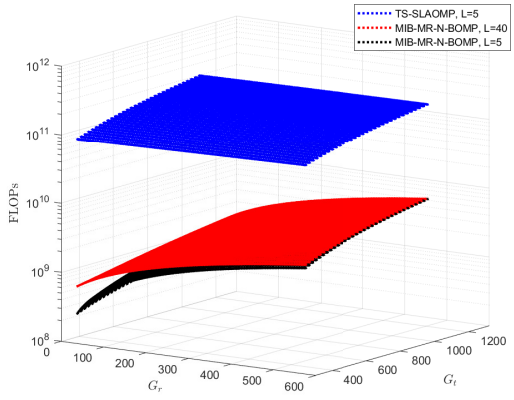

Fig. 6: Complexity of RIS-BS channel estimations.

V. Conclusion

This paper proposes the MIB-LAOMP and MIB-MR-N-BOMP for the channel estimation in the user-RIS and RIS-BS channels, respectively, for the RIS-aided communication system. The MIB-LAOMP algorithm utilizes matrix inverse bypass and look ahead strategies to reduce computational complexity. Specifically, in user-RIS channel estimation, MIB-LAOMP reduces computational complexity by 10.96% compared to LAOMP. In RIS-BS channel estimation, using the MIB-MR-N-BOMP method, the NMSE performance improved by 75.07% compared to TS-SLAOMP under SNR $=$ 10dB and $Q = 64$. Moreover, the computational complexity was reduced by 95.73% compared to TS-SLAOMP.

The final simulation and analysis results show that the proposed algorithm can achieve better performances than other state-of-art algorithms with apparent complexity reduction.

References

[1] C. Huang, A. Zappone, G. C. Alexandropoulos, M. Debbah, and C. Yuen, "Reconfigurable intelligent surfaces for energy efficiency in wireless communication," *IEEE Transactions on Wireless Communications*, vol. 18, no. 8, pp. 4157–4170, 2019.

[2] M. Di Renzo, A. Zappone, M. Debbah, M.-S. Alouini, C. Yuen, J. de Rosny, and S. Tretyakov, "Smart radio environments empowered by reconfigurable intelligent surfaces: How it works, state of research, and the road ahead," *IEEE Journal on Selected Areas in Communications*, vol. 38, no. 11, pp. 2450–2525, 2020.

[3] J. Hu, H. Yin, and E. Bjornson, "MmWave MIMO Communication with Semi-Passive RIS: A Low-Complexity Channel Estimation Scheme," in *2021 IEEE Global Communications Conference (GLOBECOM)*, 2021, pp. 01–06.

[4] E. Vlachos, G. C. Alexandropoulos, and J. Thompson, "Wideband MIMO Channel Estimation for Hybrid Beamforming Millimeter Wave Systems via Random Spatial Sampling," *IEEE Journal of Selected Topics in Signal Processing*, vol. 13, no. 5, pp. 1136–1150, 2019.

[5] R. Li, B. Guo, M. Tao, Y.-F. Liu, and W. Yu, "Joint design of hybrid beamforming and reflection coefficients in RIS-aided mmWave MIMO systems," *IEEE Transactions on Communications*, vol. 70, no. 4, pp. 2404–2416, 2022.

[6] Y. Sun *et al.*, "Energy-efficient hybrid beamforming for multilayer RIS-assisted secure integrated terrestrial-aerial networks," *IEEE Transactions on Communications*, vol. 70, no. 6, pp. 4189–4210, 2022.

[7] P. Wang, J. Fang, L. Dai, and H. Li, "Joint transceiver and large intelligent surface design for massive MIMO mmWave systems," *IEEE transactions on wireless communications*, vol. 20, no. 2, pp. 1052–1064, 2020.

[8] S. Liu, Z. Gao, J. Zhang, M. Di Renzo, and M.-S. Alouini, "Deep denoising neural network assisted compressive channel estimation for mmWave intelligent reflecting surfaces," *IEEE Transactions on Vehicular Technology*, vol. 69, no. 8, pp. 9223–9228, 2020.

[9] S. Chatterjee, D. Sundman, and M. Skoglund, "Look ahead orthogonal matching pursuit," in *2011 IEEE International Conference on Acoustics, Speech and Signal Processing (ICASSP)*, 2011, pp. 4024–4027.

[10] Y. Tian and Y. Takane, "More on generalized inverses of partitioned matrices with Banachiewicz–Schur forms," *Linear Algebra and its Applications*, vol. 430, no. 5, pp. 1641–1655, 2009, special Issue devoted to the 14th ILAS Conference. [Online]. Available: https://www.sciencedirect.com/science/article/pii/S0024379508003078

[11] C. F. Caiafa and A. Cichocki, "Computing Sparse Representations of Multidimensional Signals Using Kronecker Bases," *Neural Computation*, vol. 25, no. 1, pp. 186–220, 01 2013. [Online]. Available: https://doi.org/10.1162/NECO_a_00385

[12] T. T. Do, L. Gan, N. Nguyen, and T. D. Tran, "Sparsity adaptive matching pursuit algorithm for practical compressed sensing," in *2008 42nd Asilomar Conference on Signals, Systems and Computers*, 2008, pp. 581–587.

[13] D. Needell and J. A. Tropp, "Cosamp: iterative signal recovery from incomplete and inaccurate samples," *Commun. ACM*, vol. 53, no. 12, p. 93–100, dec 2010. [Online]. Available: https://doi.org/10.1145/1859204.1859229

[14] S. Yang, W. Lyu, D. Wang, and Z. Zhang, "Separate Channel Estimation With Hybrid RIS-Aided Multi-User Communications," *IEEE Transactions on Vehicular Technology*, vol. 72, no. 1, pp. 1318–1324, 2023.